Single-Frequency Network Terrestrial Broadcasting with 5GNR Numerology Using Recurrent Neural Network

*electronics*

MDPI

*Communication*

# Single-Frequency Network Terrestrial Broadcasting with 5GNR Numerology Using Recurrent Neural Network

**Majid Mosavat * and Guido Montorsi ***

Department of Electronics and Telecommunications, Politecnico di Torino, 10129 Turin, Italy
* Correspondence: majid.mosavat@polito.it (M.M.); guido.montorsi@polito.it (G.M.)

**Abstract:** We explore the feasibility of Terrestrial Broadcasting in a Single-Frequency Network (SFN) with standard 5G New Radio (5GNR) numerology designed for uni-cast transmission. Instead of the classical OFDM symbol-by-symbol detector scheme or a more complex equalization technique, we designed a Recurrent-Neural-Network (RNN)-based detector that replaces the channel estimation and equalization blocks. The RNN is a bidirectional Long Short-Term Memory (bi-LSTM) that computes the log-likelihood ratios delivered to the LDPC decoder starting from the received symbols affected by strong intersymbol/intercarrier interference (ISI/ICI) on time-varying channels. To simplify the RNN receiver and reduce the system overhead, pilot and data signals in our proposed scheme are superimposed instead of interspersed. We describe the parameter optimization of the RNN and provide end-to-end simulation results, comparing them with those of a classical system, where the OFDM waveform is specifically designed for Terrestrial Broadcasting. We show that the system outperforms classical receivers, especially in challenging scenarios associated with large intersite distance and large mobility. We also provide evidence of the robustness of the designed RNN receiver, showing that an RNN receiver trained on a single signal-to-noise ratio and user velocity performs efficiently also in a large range of scenarios with different signal-to-noise ratios and velocities.

**Keywords:** OFDM; channel estimation; channel equalization; data detection; neural network; RNN; LSTM; 5GNR; broadcasting



**Citation:** Mosavat, M.; Montorsi, G. Single-Frequency Network Terrestrial Broadcasting with 5GNR Numerology Using Recurrent Neural Network. *Electronics* **2022**, *11*, 3130. https://doi.org/10.3390/electronics11193130

Academic Editor: Cheng-Chi Lee

Received: 24 August 2022
Accepted: 26 September 2022
Published: 29 September 2022



## 1. Introduction

In a Single-Frequency Network (SFN) Terrestrial Broadcasting system based on Orthogonal Frequency Division Multiplexing (OFDM), all broadcasting stations simultaneously transmit the same OFDM signal over the same frequency channel. The signal propagates through different paths and reaches the receiver at separate times, creating an "artificial" delay spread. To compensate the different propagation delays and eliminate the ISI between received symbols, a Cyclic Prefix (CP) is appended to the transmitted symbol. The CP length is then designed to be greater than the echoes' temporal dispersion, which, in turn, is related to the maximum Intersite Distance (ISD) of the considered broadcasting infrastructure. Most recent Terrestrial Broadcasting OFDM standards are based on this solution, such as DVB-T2 [1] and ATSC 3.0 [2].

LTE-based Terrestrial Broadcasting has also introduced two specific carrier spacings [3] to meet the requirements of a dedicated broadcast network. The 2.5 kHz carrier spacing with a 100 µs CP length delivers mobile services to portable and handheld receivers with a 15 km ISD and a speed up to 250 km/h. The 0.37 kHz carrier spacing with a 300 µs CP length is designed for roof-top reception and up to a 175 km ISD.

In strongly double-selective scenarios, the classical approach to the OFDM design of SFNs becomes progressively inefficient for the two following reasons. On the one hand, to prevent the ISI, the CP must be kept larger than the delay spread associated with the ISD, and at the same time, the symbol duration must be kept much smaller than the channel coherence time to prevent the ICI. The ratio of the CP to the symbol duration, representing

the system energy and throughput overhead, can become unacceptable. Furthermore, the pilot density required to efficiently estimate and interpolate the channel with a small coherence bandwidth and time becomes unacceptably high, introducing a further overhead.

Fifth-Generation New Radio (5GNR) defines OFDM numerologies designed only for uni-cast transmission, with larger carrier spacing (a minimum of 15 kHz) and characterized by a rather short CP (4.7 μs). In this case, with a classical OFDM receiver, it is possible to support SFNs with a maximum of only a 5 km ISD [4], not compatible with most broadcaster infrastructures.

To support larger ISDs with 5GNR numerologies, the receiver must then be equipped with an advanced OFDM detector capable of dealing with a large ISI/ICI.

In [5], we proposed a linear 2D filter in the frequency domain for the equalization of the OFDM system in the presence of the ISI spanning several OFDM symbols. The results showed that, by using the channel shortening technique in [6], it is possible to obtain with 5GNR numerologies the same performance of OFDM systems specifically designed for SFN Terrestrial Broadcasting [3]. Those results, however, were based on a static channel and assumed the channel impulse response is known by the receiver.

In this paper, we approach the more realistic and challenging scenario, where on top of a strong ISI and ICI, due to the adoption of 5GNR numerology for SFN scenarios, the considered channel is very rapidly time-varying (mobile speed up to 200 km/h) and unknown to the receiver.

In the literature, the investigation of advanced receiver techniques for the compensation of the ISI/ICI in an OFDM system is broad, but limited to specific scenarios. For ADSL systems, which are characterized by quasi-static channels, the authors of [7] proposed an approach to compensate the effect of the channel within the CP in a static channel condition. In [8,9], the authors proposed low-complexity equalizers for video broadcasting in time- and frequency-selective channels, although the considered CP length was larger than the delay spread. The authors in [10] studied a one-tap decision feedback equalizer for an OFDM system with the ISI and ICI, but in a low-mobility environment. The authors of [11] designed a more complex system for a doubly dispersive multi-carrier system and focused on a large delay spread with an embedded channel encoder. The delay spread was within the OFDM symbol. Notice that most of these papers assumed channel state information is known by the receiver, a very strong assumption, especially in a mobile environment. Furthermore, in the literature on OFDM for the wireless channel, the amount of ISI is typically limited within one symbol period, while, in our problem, statement, it can last several OFDM symbols. While the adoption of advanced equalization techniques may eliminate the CP inefficiency by removing the constraint on the CP and symbol duration, the second source of inefficiency due to the required pilot density for channel estimation cannot be eliminated.

In this paper, we consider a more recent approach, where the totality or part of the receiver structure is substituted by the RNN. RNNs offer an impressive capability of adapting their behavior to solve very complex inference problems, and they have the ability to learn and extract information from time series [12]. In this research, for the first time, we used an RNN, bidirectional Long Short-Term Memory (bi-LSTM), in processing the 5GNR waveform to enable Terrestrial Broadcasting.

bi-LSTM [13] is a special kind of RNN composed of two chains of concatenated LSTM cells to which the data sequence is fed, once forward and once backward, and finally, concatenated. The structure is similar to that of the BCJR algorithm for maximum likelihood detection, where forward and backward recursions are performed to extract information from the past and future observations relevant for the target variable to be estimated. Each LSTM cell is composed of an input gate, forget gate, output gate, and one candidate memory cell [14].

The ability of the RNN to process time sequences was investigated also in the context of signal processing. For instance, the authors of [15] proposed a Sliding Bidirectional Recurrent Neural Network (SBRNN) for single-carrier real-time sequence detection. The

authors of [16] introduced a scheme for joint channel estimation and symbol detection for an OFDM system. The work in [17] proposed a deep-learning-assisted technique for signal detection in the up-link and fast time-varying channel with bi-LSTM. In [18], the authors proposed a neural network architecture named Cascaded Net (CN) for OFDM symbol equalization.

To the best of our knowledge, in the RNNs that have been proposed in the past for OFDM systems, the authors either assumed the channel impulse response length within the CP length (no ISI) or they did not investigate the OFDM symbol affected by the ISI and time-varying channel jointly. Furthermore, the authors used the classical OFDM approach for assigning specific resources for channel estimation, causing a large amount of overhead to be imposed on the system, especially in situations where the speed of the receiver is high and a dense pilot map is required. In most cases, the authors did not consider the presence of an outer forward error correction technique, e.g., Low-Density Parity Check Code (LDPC), and directly reported the bit error rate at the output of the detector as the key performance indicator.

To remove the two sources of inefficiency, due to the excessive CP length and pilot density, we propose a novel approach that embeds two solutions:

1. Replacement of the channel estimator, channel equalization, and LLR computation blocks with a recurrent neural network block;
2. Usage of superimposed pilots instead of interspersed pilots.

In the proposed receiver, the RNN detector is placed after the FFT and before the LDPC decoding. By suitably training it offline, the designed RNN receiver shows the appropriate flexibility to face rapid channel changes and strong ISI/ICI in a wide set of scenarios. The paper presents the detail of the careful optimization procedure of the RNN that led to the final design.

The rest of this paper is organized as follows. In Section 2, we provide the details of the considered channel models for the SFN scenario and the description of the reference classical OFDM system. We then describe our proposed receiver based on the RNN detector and superimposed pilots, discussing its complexity. In Section 3, we optimize the hyper-parameters of the proposed RNN detector for two SFN infrastructures. In Section 4, we present end-to-end simulation results comparing and discussing the performance of the proposed approach with that of the reference system. Conclusions follow in Section 5.

## 2. Reference System and Proposed Approach with RNN and Superimposed Pilots

The considered OFDM system for Terrestrial Broadcasting in an SFN is shown in Figure 1. In the following sections, we provide the details on the channel model, the reference classical system, and the proposed approach, which includes the superposition of the pilots and the adoption of the RNN in a part of the receiver (modification highlighted in red in Figure 1).

### *2.1. Channel Model for SFN*

The transmitted signal is sent through a Tapped Delay Line (TDL) channel model, which is characterized by its maximum delay spread. The considered TDL channel model (TDL-A) is the standard one defined in [19]. TDL-A is a challenging channel model for a non-line-of-sight environment. It is used also for modeling an SFN by properly scaling its maximum delay spread according to the considered ISD. In Table 1, we report the correspondence between the maximum delay spread in the TDL-A model and the considered ISD in the SFN for Low-Power Low-Tower (LPLT), Medium-Power Medium-Tower (MPMT), and High-Power-High Tower (HPHT) transmission networks.

**Table 1.** Correspondence between maximum delay spread and intersite distance for modeling SFNs.

| Parameter | LPLT | MPMT | HPHT |
|---|---|---|---|
| ISD (km) | 15 | 50 | 125 |
| Delay spread (μs) | 20 | 40 | 50 |

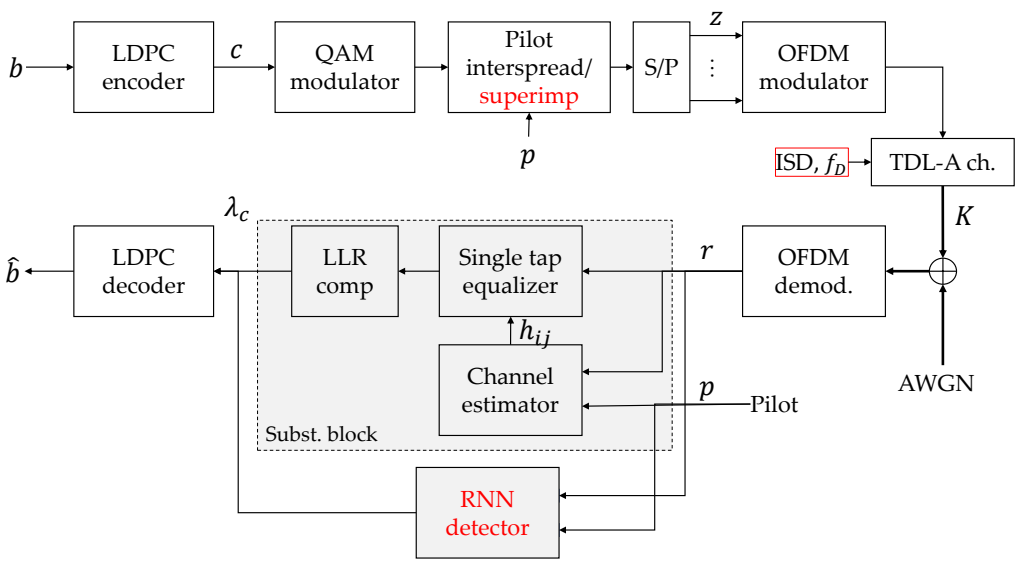


**Figure 1.** The OFDM system and position of the proposed RNN detector.

In all considered scenarios, we fixed the number of receiver antennas to $K = 2$ and the carrier frequency to $f_0$ = 700 MHz, a common choice for broadcasting. The considered maximum user speed is $v = 200$ km/h, corresponding to a maximum Doppler frequency $f_D = \frac{c}{v} f_0 = 129$ Hz, with Jake's model for the spectrum of tap coefficients.

### 2.2. Classical Terrestrial Broadcasting in SFN

The stream of information bits $b$ generated by the source is encoded by the channel encoder [20], producing the sequence of coded bits $c$. The encoded bits are converted to complex signals by the QAM modulator. For channel estimation, a properly designed pilot sequence $p$ is *interspersed* with the information signals. The $N$ parallel frequency domain signals are converted to the time domain via the Inverse Fast Fourier Transform (IFFT), and the CP with a suitable length is inserted to prevent the ISI (OFDM modulator block).

At the receiver side, time domain signals are received by $K$ antennas. The OFDM demodulators, one for each receiving antenna, convert time domain signals to $N$ parallel frequency domain signals. A pilot-assisted channel estimation is carried out using the transmitted pilot symbols. The considered channel estimation algorithm in the reference receiver uses least-mean-squares estimation and linear interpolation to obtain the channel gains on data subcarriers. A single tap equalizer is then used to provide the equalized signal. The LLR computation block calculates log-likelihood ratios on coded bits $\lambda_n$ at time $n$, and the LDPC decoder processes the LLR to provide estimated bits $\hat{b}$.

It is well known that the performance of this simple receiver scheme is directly connected to the trade-offs between the CP length, channel delay spread, carrier spacing, and user mobility. In the standard design of OFDM numerology, the CP length is kept larger than the delay spread to prevent the ISI and OFDM symbol duration $1/\Delta f$ is kept much smaller than the channel coherence time to prevent the ICI.

The 5GNR numerology with a short or very short OFDM symbol length makes possible the symbol-by-symbol detection of the OFDM symbol even with a high speed. However, the short CP length (4.7 μs) of the 5G OFDM symbol is not compatible with the large ISD of the Terrestrial Broadcasting scenario (see Table 1). The delay spread of SFN environments

makes each transmitted OFDM symbol interfere with *several* contiguous OFDM symbols. The ISI between OFDM symbols destroys the orthogonality of carrier spacing, and the ICI occurs. Terrestrial Broadcasting with 5GNR numerology becomes impossible with the classical data detection scheme.

### *2.3. The Proposed Approach*

The blocks highlighted in red in Figure 1 summarize the proposed modifications to the reference system.

#### 2.3.1. Superimposed Pilots

One major obstacle in adopting the RNN structure is that of properly exploiting the pilot sequence information that is provided as side information at the receiver for performing the required channel estimation task. When using pilot sequences interspersed with data symbols, the classical receiver exploits the knowledge of pilot positions to perform different operations at different time/frequency resources. Channel estimation is performed on pilot resources, while equalization, exploiting the channel estimation results, is performed on data resources. This non-stationary behavior of the classical receiver is incompatible with the RNN structure, which is intrinsically stationary, and information about the pilot position is difficult to embed in such structures. For this reason, at the transmitter side, instead of using the typical interspersing pilot technique, pilot and data signals are **superimposed**. The superimposed pilot approach has been already proposed and studied in advanced receivers [21]. At the price of introducing cross-interference between the data and pilots, it offers several advantages. No bandwidth overhead for channel estimation is introduced as all resources are assigned to data, and at the same time, pilot information is available at all resources for channel estimation. The cross-interference between the data and pilot, on the other hand, can be suitably removed by advanced cancellation techniques. In our case, this approach also circumvents the problem of exploiting the information on the pilot position at the RNN detector.

At the transmitter side, with superimposed pilots, the transmitted symbol at time $n$ on carrier $m$ is obtained as:

$$z_{mn} = d_{mn}\sqrt{1-\alpha^2} + p_{mn}\alpha \tag{1}$$

where $d_{mn}$ is the data symbol and $p_{mn}$ the pilot symbol. The single parameter $\alpha$ controls the assigned energy ratio for the pilot and data signal.

#### 2.3.2. A Recurrent Neural Network Detector for SFN Terrestrial Broadcasting

In our proposed receiver in Figure 1, we substituted three blocks of the OFDM detector (channel estimator, channel equalizer, and LLR computation) with one RNN block.

The details of the RNN receiver are shown in Figure 2. The RNN includes two layers of bi-LSTM, two dropout layers, and one output dense SoftMax for delivering the bit log-likelihood vector.

With $K$ receiving antennas, the demodulated OFDM symbol vector becomes $r_n = [r_{11}, \ldots, r_{1N}, \ldots, r_{K1}, \ldots, r_{KN}]_n$, and the vector of reference known pilots is denoted by $p_n = [p_1, \ldots, p_N]_n$. The available observation vector at time $n$ at the RNN input is then the real vector $y_n = [\Re[r_n, p_n], \Im[r_n, p_n]]$ with size $2(K+1) \cdot N$.

As transmission is affected by the ISI, $M$ consecutive OFDM symbols are included for the data estimation, so that the input vector at time $n$ to the RNNs is given by:

$$\bar{\mathbf{y}}_n \triangleq \left[ y_{n-\lfloor \frac{M}{2} \rfloor}, \ldots, y_n, \ldots, y_{n+\lfloor \frac{M}{2} \rfloor} \right]. \tag{2}$$

The complexity and representation capability of bi-LSTM is controlled by the number of LSTM cell units ($U$), which also corresponds to the size of the output of each LSTM cell. The dropout layer is one regularization technique that is used only during network training

and prevents overfitting [22]. The dense layer maps the output of the previous layer to the dimensionality of the output space, which consists of $N \times n_b$ bit log-likelihood ratios:

$$\lambda_i = \ln\left(\frac{q_i}{1-q_i}\right), \tag{3}$$

where $q_i$ is the $i$-th predicted probability of symbol "1".

To train the RNN detector, we generated $S$ pairs of $\bar{\mathbf{y}}_n$ and their target coded bits $c_n$. At each stage of one training epoch, $B$ pairs (a batch) from $S$ pairs are selected randomly and forwarded to the RNN detector. We calculated the error between the target and actual response of the RNN detector with the binary cross-entropy loss function, which is given by:

$$\delta = -\frac{1}{B}\frac{1}{N \cdot n_b}\sum_{j=1}^{B}\sum_{i=1}^{N \cdot n_b}[c_{ij} \cdot \log q_{ij} + (1-c_{ij}) \cdot \log(1-q_{ij})], \tag{4}$$

where $B$ is the batch size and $c_{ij}$ is the target bit value. The error $\delta$ is then backpropagated along the network, revising the weights via the gradient descent algorithm [23]. This operation is repeated $\frac{S}{B}$ times, and one epoch ends. In the next epoch, each batch is randomly created again, from the same set of $S$ pairs, and the operation is repeated until an acceptable level of entropy is achieved at the end of an epoch.

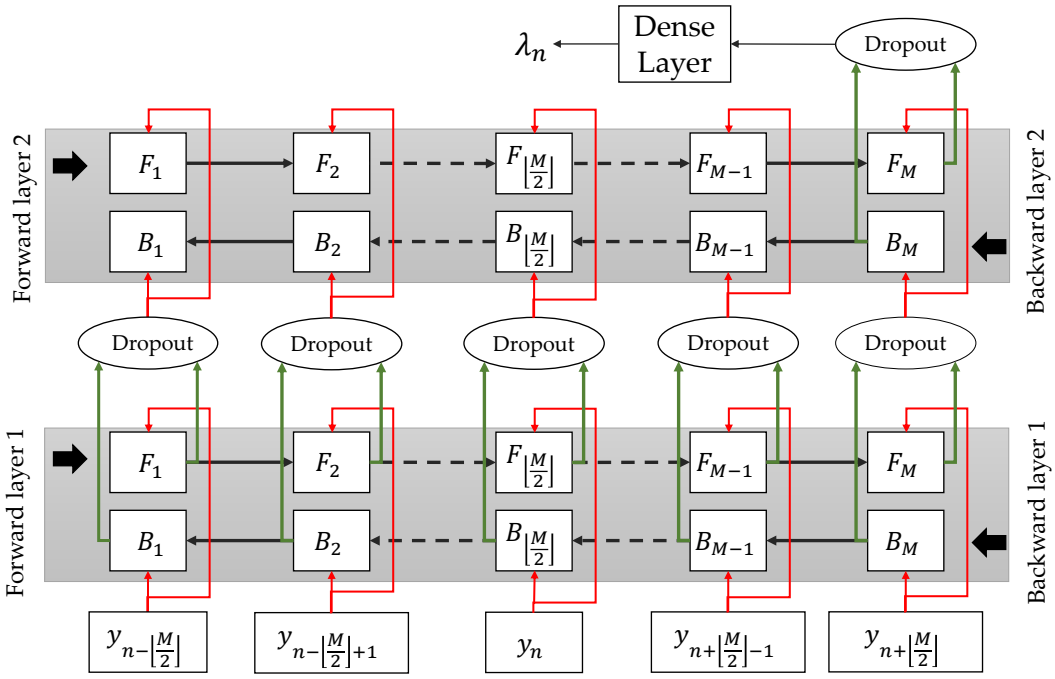


**Figure 2.** Unrolled RNN detector for an OFDM system ($M$ is odd).

#### 2.3.3. Discussion on RNN Detector Complexity

One of the major issues that prevents the adoption of RNNs as a substitute of the classical receiver structure is their complexity. The number of operations in each of the $M$ cells in a single layer of bi-LSTM ($F$), corresponding to the number of trainable parameters, is given by:

$$F = 2 \times 4 \times (I \times U + U^2 + U), \tag{5}$$

where $I$ is the size of the input vector to each bi-LSTM layer. In our RNN in Figure 2, $I = 2(K+1) \cdot N$ for the first layer and $I = 2 \cdot U$ for the second layer. The complexity of the RNN increases then linearly with the increasing size of input vector $I$ and the sequence length $M$, but quadratically with the number of units. The output dense layer complexity amounts to $n_b \times 2 \times U$ and is negligible. In this study, we fixed the number

of units to $U$ = 400 based on the work of [17]; all optimizations were performed based on this value, but according to further results presented in the final section of Table 2, similar entropy losses were obtained using lower values for the number of units. Using $U = 100$, although the training time increased, the performance became slightly better. In this case, the complexity of the system was reduced by a factor 1/16.

## 3. Optimization of RNN

In this section, we define the system parameters of the RNN. Then, the RNN parameters are optimized separately for one LPLT and one HPHT network.

### *3.1. RNN System Parameters and Preliminary Data Generation for Training*

For the RNN, we considered a system with 12 OFDM carriers with a carrier spacing of 15 kHz, yielding a system bandwidth of 180 kHz (one resource element in 5G New Radio) for link-level simulations. This small bandwidth was chosen to facilitate the RNN training process and can be increased to practical values for broadcasting, such as 10 MHz, in which case, the complexity of the receiver increases linearly by replicating the RNN detector for each resource block.

The OFDM symbol length is 71 µs, including the normal CP (4.7 µs). We used the 4-QAM constellation ($n_b = 2$) corresponding to 24 coded bits transmitted per symbol.

The TDL-A channel model has 20 µs and 50 µs delay spreads, which are standard values for emulating LPLT and HPHT networks with 15- and 125-kilometer ISDs (see Table 1). We fixed the number of receiver antennas to $K = 2$ and the carrier frequency to 700 MHz. The receiver speeds used for generating the training pairs were equal to 160 km/h for LPLT and 3 km/h for HPHT, which make the maximum Doppler shift around 103 and 3 Hz, respectively. Ten million pairs $(y_n, c_n)$ at a fixed SNR = 5 dB were generated for parameter optimization and offline training, one for the LPLT network and one for the HPHT network. The ADAM optimizer [24] was used for training the RNN detector with a learning rate of 0.001. At the end of the training phase, we then generated two RNNs, one trained at 160 km/h for LPLT and one trained at 3 km/h for HPHT. These two RNNs are those used in all results reported in the final section. The Matlab platform was used to generate the input data sequences and output labels of the RNN. The RNN training was performed using Keras, a Python interface for the *Tensorflow* library. The trained RNN was then imported into MATLAB to check the system end-to-end performances.

### *3.2. RNN Preliminary Hyper-Parameter Optimization for LPLT Network*

The target free hyper-parameters for optimizing the proposed RNN system are the value of $\alpha$ for pilot superposition, the length $M$ of the input vector to the RNN, and the batch size $B$ used for training. In the preliminary optimization step, we randomly generated 100 k arrays of $\bar{\mathbf{y}}_n$ with SNR = 5 dB and speed 160 km/h, each with size $M$, and corresponding target bits $c$ from the data pairs created in the previous step. We then trained the network with 90 k arrays of $\bar{\mathbf{y}}_n$, and the trained RNN detector was tested with the final 10 k of $\bar{\mathbf{y}}_n$.

Some relevant results of the optimization campaign are reported in Table 2 for the LPLT network. In the second column of the table, we report the minimum binary cross-entropy ($\delta$), and in the third column, the epochs were the minimum reached, to show the amount of time required for optimization.

Fixing $B$ = 4096 and $M$ = 15, the assignment $\alpha = 0.5$ provided minimum cross-entropy loss for the test data sequences.

Regarding the optimization of the length of the input observation window $M$, since the RNN performs both tasks of channel estimation and equalization, $M$ is expected in general to be related to both the coherence time of the channel and the delay spread. In our scenario, having fixed $\alpha = 0.5$ and $B = 4096$, the best trade-off was obtained for $M$ = 15.

We finally examined the effect of batch size $B$ for the RNN detector, with $M = 15$ and $\alpha = 0.5$. Training the RNN detector with a larger batch size provided a lower binary cross-entropy loss.

Based on this initial parameter optimization, in the final RNN, we set $\alpha = 0.5$, $B$ = 4096, $M$ = 15, dropout to 0.5, and $U$ = 400. To improve the performance, we increased the training set $S$ to two million for each epoch, keeping the final 10k pairs for testing (last line in Table 2).

Considering that the RNN complexity is driven by the value of $U$, we also checked the network performance by reducing $U$. Results are reported in the third part of Table 2. It turned out that, in this case, reducing $U$ may require a longer training time (third column of the table), but can lead to a network with better performances and lower complexity.

**Table 2.** RNN parameter optimization. Minimum binary cross-entropy loss of the validation data set for the LPLT SFN.

| Parameters | Minimum Loss ($\delta$) | Minimum Epochs |
|---|---|---|
| $\alpha = 0.25$ | 0.4043 | 33 |
| $\alpha = 0.5$ | **0.3774** | 32 |
| $\alpha = 0.75$ | 0.442 | 40 |
| $M = 7$ | 0.3953 | 38 |
| $M = 15$ | **0.3774** | 32 |
| $M = 21$ | 0.3972 | 38 |
| $B = 64$ | 0.3921 | 20 |
| $B = 256$ | 0.3839 | 15 |
| $B = 4096$ | **0.3774** | 20 |
| $U = 400$ | 0.3774 | 32 |
| $U = 200$ | 0.3576 | 96 |
| $U = 100$ | **0.3481** | 271 |
| final LPLT RNN | **0.25** | 56 |

### *3.3. RNN Hyper-Parameter Optimization for HPHT Network*

The described LPLT parameter optimization was repeated for the HPHT network (see Table 3). In this case, the SNR was still fixed to 5 dB and the speed was set to 3 km/h.

We optimized parameter $\alpha$ with $M = 9$, $B = 4096$, and $U = 400$. The minimum cross-entropy loss was obtained with $\alpha$=0.5, which is the same result obtained for the LPLT network. Then, we optimized $M$ fixing $\alpha = 0.5$. The value $M$ = 9 provided the best performance.

Due to the larger delay spread, as expected, the minimum loss obtained for HPHT was larger than that obtained for the LPLT RNN. For training the final network, setting $M = 9$, $\alpha$ = 0.5, $B$ = 4096, and $U$ = 400, we increased $S$ to three million (last line of Table 3).

**Table 3.** RNN parameter optimization. Minimum binary cross-entropy loss of the validation data set for the HPHT SFN.

| Parameters | Minimum Loss ($\delta$) | Minimum Epochs |
|---|---|---|
| $\alpha = 0.25$ | 0.5057 | 27 |
| $\alpha = 0.5$ | **0.3926** | 32 |
| $\alpha = 0.75$ | 0.415 | 37 |
| $M = 7$ | 0.4067 | 33 |
| $M = 9$ | **0.3926** | 32 |
| $M = 11$ | 0.3952 | 30 |
| $M = 13$ | 0.3939 | 31 |
| $M = 15$ | 0.3931 | 31 |
| $M = 17$ | 0.3973 | 30 |
| $M = 19$ | 0.4009 | 29 |
| $M = 21$ | 0.4099 | 32 |
| final HPHT RNN | **0.28** | 56 |

## 4. End-to-End Simulations Compared to a Reference Classical System

In this section, we present the performance of the two RNNs optimized in the previous section against a classical reference system, whose system parameters are described in the next subsection.

### *4.1. Classical Reference System Numerologies and Pilot Signals*

The Third Generation Partnership Project (3GPP) specified two numerologies in Long-Term Evolution (LTE) evolved Multimedia Broadcast Multi-cast Service (eMBMS) to address the requirements of a dedicated broadcast network. The first one, with a carrier spacing of 2.5 kHz with a 100 µs CP length, is designed for the LPLT SFN with a maximum ISD of 15 km. This solution provides high mobility supporting up to 250 km/h for broadcasting scenarios.

The second one, with a carrier spacing of 0.37 kHz and a 300 µs CP length, is designed to support the conventional HPHT SFN up to a 175 km ISD, targeting *fixed* roof-top reception. The performances of these systems in some typical broadcasting scenarios are available in [3,25].

Using the fixed bandwidth of 180 kHz considered for the RNN-based system, the number of carriers for the two systems is $N = 180/2.5 = 72$ and $N = 180/0.37 \approx 486$, respectively.

The suggested pilot pattern in [26] to support the time-varying characteristic of the TDL-A channel requires 1 out of 4 resources allocated for the pilots, with pilot resource frequency spacing $F_d = 2$ and time spacing $T_d = 2$. These values are reduced to 1 out of 6 in the roof-top scenario ($F_d = 3$, $T_d = 2$).

### *4.2. End-to-End Simulation for LPLT and HPHT SFN*

The transmitted information throughput $T$ (bits/s) of an OFDM system can be written as

$$T = R_s \times n_b \cdot N \times (\eta \times r_c), \tag{6}$$

where $R_s$ is the OFDM symbol rate, $\eta$ is the waveform efficiency, a factor smaller than one that accounts for the system overhead, and $r_c$ is the code rate. The values of the parameters in Equation (6) differ for the two considered systems due to the different strategies for pilot insertion and different CP overheads. In our RNN system, the overhead is only due to the 5GNR CP insertion, and the efficiency amounts to $\eta_{RNN} = 15/16 = 0.9375$; for the LPLT reference system, it is the product of the CP efficiency (400 µs/500 µs) and the pilot efficiency 3/4, so that, overall, the efficiency is $\eta_C = 0.6$.

To have a fair performance comparison, we fixed the same throughput, so that we adjusted the code rate $r_c$ of the two systems to have a fixed product $\eta \times r_c$:

$$r_c^{(C)} \eta_C = r_c^{(RNN)} \eta_{RNN} \rightarrow r_c^{(C)} = 1.5625 \cdot r_c^{(RNN)}.$$

The performance comparison of the two systems (RNN system with 15 kHz 5GNR numerology, classical system with 2.5 kHz), in terms of the BER at the output of the 5GNR LDPC decoder, is shown in Figure 3. For both systems, we used an LDPC encoder with codeword block size 20k and a layered LDPC decoder with 25 iterations.

We report results with two target throughputs T1 = 114 kbit/s and T2 = 162 kbit/s. For T1, the corresponding code rate for the RNN system is $r_{c,1}^{(RNN)} = 0.34$ and that required for the reference classical system is $r_{c,1}^{(C)} = 0.53$. For T2, $r_{c,2}^{(RNN)} = 0.48$ and $r_{c,2}^{(C)} = 0.75$.

The results acquired for the classical system are aligned with the results found in [25] for similar scenario settings. At BER = $10^{-3}$, the RNN provides a gain of 2 dB for T1 and a gain of 4 dB for T2. Notice that the RNN system with larger throughput T2 (green curve) also outperforms the classical system with lower throughput T1 (blue curve). Although the receiver was trained at SNR = 5 dB, its performance remained excellent at different SNR values.

We also investigated the flexibility of the designed RNN, trained at a fixed speed of 160 km/h and SNR = 5 dB, for other mobile speeds. The results are depicted in Figure 4 for the same throughput of 138 kbit/s, corresponding to $r_c^{(RNN)} = 0.41$ and $r_c^{(C)} = 0.64$.

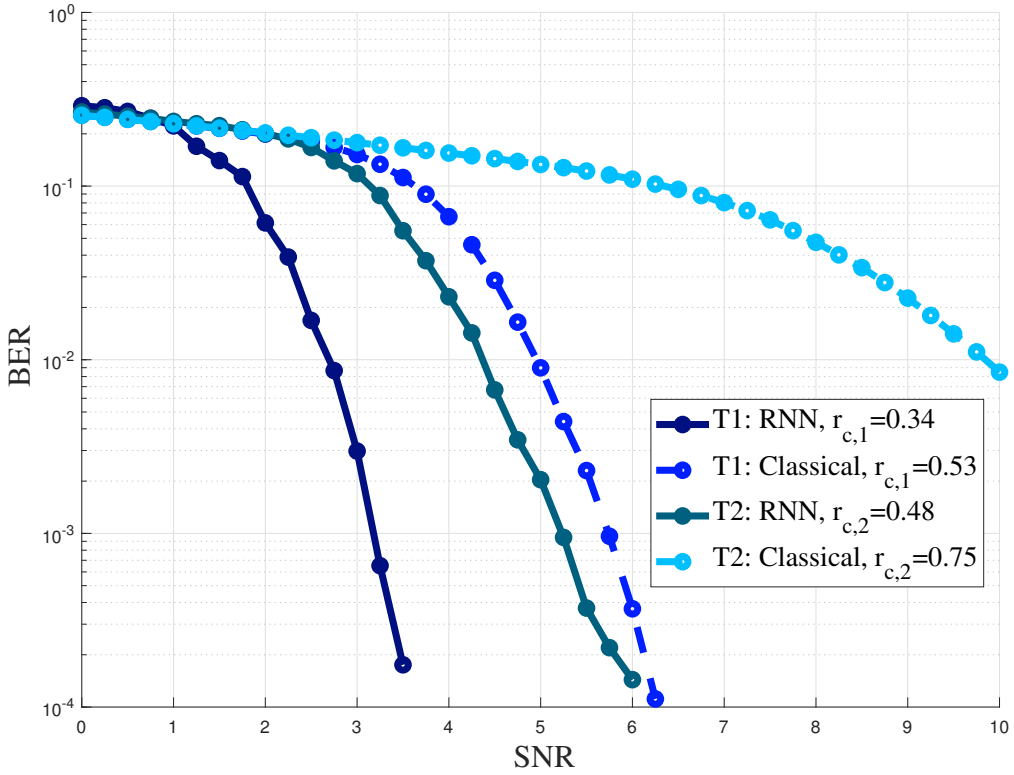


**Figure 3.** LPLT (ISD = 15 km). Performances of the RNN vs. classical Terrestrial Broadcasting system with two throughputs (T1 = 114 kbit/s, T2 = 162 kbit/s) and a fixed speed of 160 km/h.

The RNN receiver performed better than the classic receiver at all speeds. The results showed that the RNN receiver, in addition to flexibility under different SNRs, has also high flexibility with respect to user mobility.

We evaluated the performance of the second trained HPHT RNN and compared it with that of the second classical system designed for the HPHT scenario and a speed of 120 km/h. In this case, the pilot efficiency of the classical system increased to 5/6 and the CP efficiency to 2700/3000, so that its waveform efficiency increased to $\eta = 0.75$.

The end-to-end simulation results for throughput systems T1 = 93 kbit/s and T2 = 110 kbit/s are depicted in Figure 5. For the first throughput T1, the RNN code rate was $r_{c,1}^{(RNN)} = 0.276$ and the classical system code rate was $r_{c,1}^{(C)} = 0.34$. For the second throughput T2, $r_{c,1}^{(RNN)} = 0.34$ and $r_{c,2}^{(C)} = 0.41$.

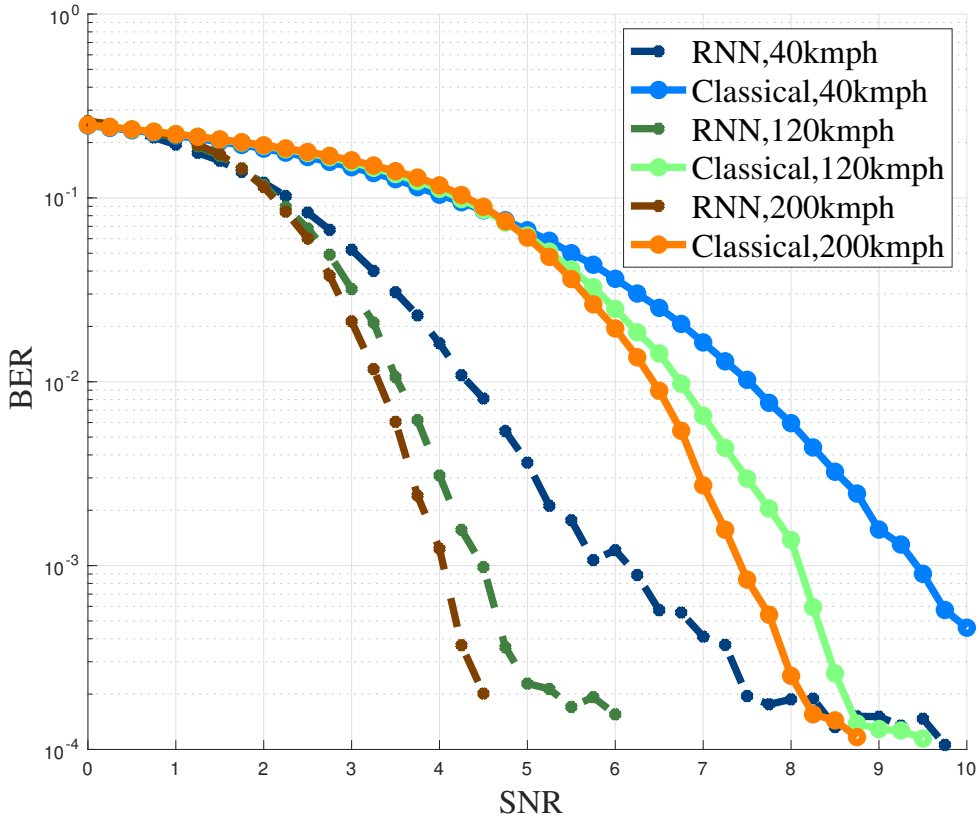


**Figure 4.** LPLT (ISD = 15 km). Performances of the RNN vs. classical Terrestrial Broadcasting system for the same throughput (138 kbit/s) and different user speeds. $r_c^{(RNN)} = 0.41$ and $r_c^{(C)} = 0.64$.

In this case also, the result showed that the RNN system outperformed the classical system, although the gain was reduced because of the increased efficiency of the classical system. At BER = $10^{-3}$, 1.2 dB and 2.3 gains were observed for T1 and T2, respectively.

Although we trained the RNN at a fixed velocity (3 km/h) and a fixed SNR (5 dB), also in this case, the RNN showed robustness at a high speed (120 km/h) and different SNRs. Notice that the classical system in this case was designed for fixed roof-top reception. No numerologies in eMBMS are provided for HPHT and mobile users. Its performances were still reasonable at 120 km/h for low-order modulation. The system however would provide unacceptable losses for higher-order modulation, due to the excessive symbol length (3 ms), incompatible with the time coherence of the channel.

The classic system can provide near-optimal performance for an SFN with a symbol-by-symbol detector by properly adjusting the OFDM length and proper allocation of the CP and pilot signals. In the classical approach, the OFDM numerology is designed to avoid the ISI and ICI and the pilot density is chosen to achieve a satisfactory channel estimation. This approach, however, becomes inefficient in the considered scenarios wherethe same delay spread is very large (HPHT) and the coherence time is small due to the user mobility.

The simulation results showed that a single trained network has great flexibility with respect to both the SNR and user speed. For HPHT, the network trained at 3 km/h provided excellent results at 120 km/h. For LPLT (see Figure 4), the trained network at 160 km/h provided excellent performance for a large set of speeds.

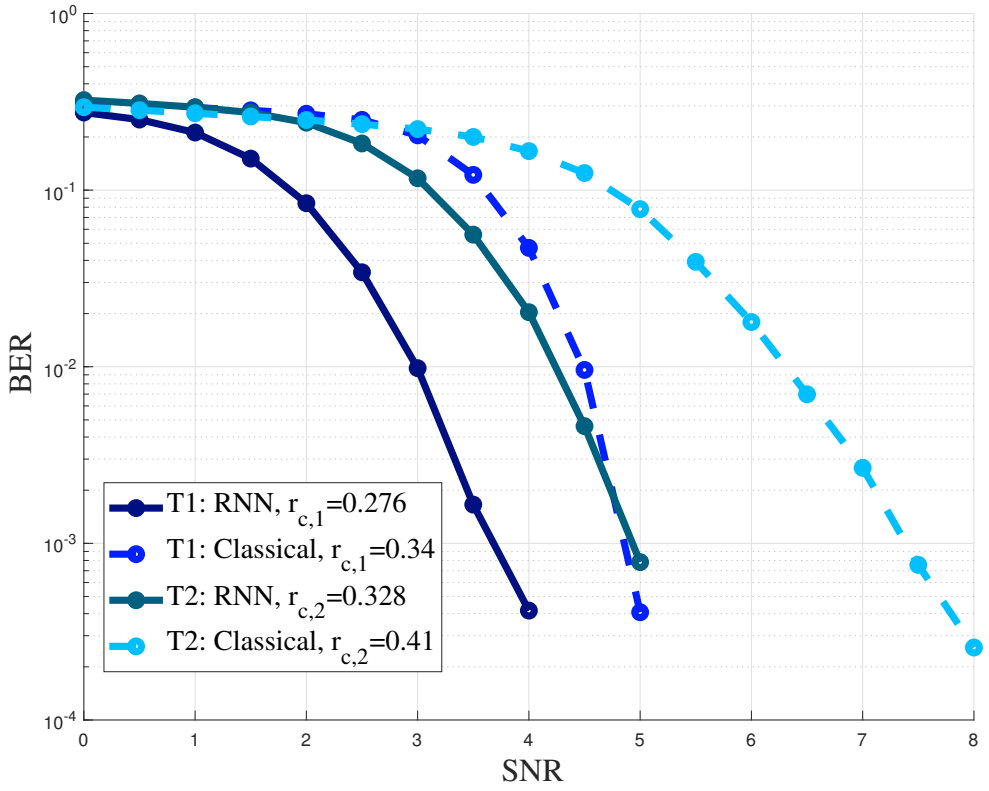


**Figure 5.** The end-to-end simulation for different throughput systems (T1 = 93 kbit/s) and (T2 = 110 kbit/s) at a fixed speed of 120 km/h and a large ISD (125 km ISD). The RNN with 5GNR numerology and trained at 3 km/h and the classical system with a 0.37 kHz carrier spacing with a long cyclic prefix of 300 µs.

## 5. Conclusions and Future Work

In this paper, we investigated the use of an RNN-based detector to support SFN Terrestrial Broadcasting. We considered the very challenging scenario where the 5GNR OFDM numerology with a short cyclic prefix (4.7 µs) and large carrier spacing (15 kHz) is used in SFN scenarios characterized by a very large delay spread (up to 50 µs). Furthermore, we considered high mobility scenarios with an unknown channel at the receiver, so that, also, channel estimation was critical.

The importance of this research comes from the fact that it is not possible to meet the requirements of SFN Terrestrial Broadcasting with the current 5GNR numerology and a classical symbol-by-symbol OFDM receiver. The possibility of using the existing 5GNR numerology for delivering broadcasting services from SFN infrastructures is indeed of great importance for broadcasters.

Previous research on SFNs mostly focused on the design of the classical OFDM system, with an ISI-/ICI-free symbol-by-symbol detection scheme. They designed new numerologies, cyclic prefix lengths, and pilot signals based on new SFN scenarios. Results on advanced, but "classical" techniques for SFNs with 5GNR numerology are not available in the literature, to our knowledge.

We proposed two ingredients for the solution, the superposition of pilots on the data at the transmitter to eliminate the pilot overhead in largely selective channels and the adoption of a suitably trained RNN at the receiver to deal with the large ISI and ICI at the receiver. The superposition of pilots also allowed us to efficiently use and train the RNN. The proposed RNN structure includes two cascaded bi-LSTM networks. In our solution, the RNN substitutes the channel estimation and equalization blocks, while the powerful outer LDPC channel decoder is kept as part of the receiver structure. The RNN thus provides the bit log-likelihood ratio to the following decoder, and the cost function

for training the RNN is changed accordingly. The hyper-parameters of the proposed RNN were optimized for generating two trained RNNs for the LPLT and HPHT SFN scenarios.

While some advanced equalizer solutions and even RNN-based receivers were proposed in past literature for OFDM, no one has considered the full problem related to the SFN as we stated, and no one has investigated the combined approach of the superposition of pilots and an RNN to solve the channel estimation and equalization problem.

We compared the end-to-end performances of the proposed approach with respect to the classical approach, used in OFDM standards such as DVB-T and ATSC. In the classical approach, OFDM numerology is designed to avoid the ISI and ICI and pilot density is chosen to achieve a satisfactory channel estimation. This approach becomes progressively inefficient in the considered scenario, where, at the same time, the delay spread is very large (HPHT) and the coherence time is small due to the user mobility. We used as the key performance indicator the BER after LDPC decoding and, consequently, that delivered to the end user. This KPI is the most relevant one in the evaluation of the physical layer, and the reported gains translate into energy savings and/or a throughput increase for the broadcasters.

The proposed approach largely outperforms the classical system, explicitly designed for the considered SFN scenarios, in all mobile scenarios. We also demonstrated the flexibility of the proposed scheme in different scenarios, as we provided evidence that a single RNN, trained at a fixed SNR and user speed, provides excellent performances in large ranges of SNRs and user speeds.

Possible future investigations related to the considered problem include:

- Adoption for a mobile SFN with 5GNR numerology of other types of advanced, but classical receivers, maybe combined with pilot superposition to increase the system efficiency.
- Reduction of the complexity of the RNN. The proposed structure based on bi-LSTM is well suited for the receiver, but probably oversized, as it was proposed for solving more complex problems. A deeper investigation of the required RNN features would probably lead to simpler structures together with a better understanding of the relationships of the RNN with the classical advanced receivers based on the MMSE and MLSE.
- The investigation of system performance with higher-order modulations, yielding higher spectral efficiencies.
- The scaling of the proposed receiver solution to the practical bandwidth used in broadcasting.
- The flexibility of a single trained RNN also for different network infrastructures (i.e., ISD) and, consequently, different delay spreads.

**Author Contributions:** M.M. designed the experiments and algorithms and wrote the draft of the manuscript. G.M. participated in the revision and discussion of the manuscript. All authors have read and agreed to the published version of the manuscript.

**Funding:** This research received no external funding.

**Institutional Review Board Statement:** Not applicable.

**Informed Consent Statement:** Not applicable.

**Data Availability Statement:** Not applicable.

**Acknowledgments:** This work is supported by RAI—Radiotelevisione Italiana Centre for Research. The authors would like to thank Vittoria Mignone and Assunta De Vita at RAI for their suggestions and contributions.

**Conflicts of Interest:** The authors declare no conflict of interest.

## References


1. Jokela, T.; Tupala, M.; Paavola, J. Analysis of physical layer signaling transmission in DVB-T2 systems. *IEEE Trans. Broadcast.* **2010**, *56*, 410–417.
2. Fuentes, M.; Mi, D.; Chen, H.; Garro, E.; Carcel, J.L.; Vargas, D.; Mouhouche, B.; Gomez-Barquero, D. Physical layer performance evaluation of LTE-advanced pro broadcast and ATSC 3.0 systems. *IEEE Trans. Broadcast.* **2018**, *65*, 477–488.
3. 3GPP TR 36.776. Evolved Universal Terrestrial Radio Access (E-UTRA); Study on LTE-Based 5G Terrestrial Broadcast. Technical Specification (ts), 3rd Generation Partnership Project (3GPP), 2020; p. 11. Version 16.0.0. Available online: https://www.etsi.org/deliver/etsi_tr/136700_136799/136776/16.00.00_60/tr_136776v160000p.pdf (accessed on 23 September 2022).
4. Gimenez, J.J.; Carcel, J.L.; Fuentes, M.; Garro, E.; Elliott, S.; Vargas, D.; Menzel, C.; Gomez-Barquero, D. 5G new radio for terrestrial broadcast: A forward-looking approach for NR-MBMS. *IEEE Trans. Broadcast.* **2019**, *65*, 356–368.
5. Mosavat, M.; Montorsi, G. Single Frequency Network Broadcasting with 5GNR Numerology. In Proceedings of the 2021 IEEE Latin-American Conference on Communications (LATINCOM), Santo Domingo, Dominican Republic, 17–19 November 2021; pp. 1–6.
6. Rusek, F.; Prlja, A. Optimal channel shortening for MIMO and ISI channels. *IEEE Trans. Wirel. Commun.* **2011**, *11*, 810–818.
7. Fatima, B. The Channel Shortening comparison between OFDM & MC-CDMA System over an ADSL Channel using a Water-filling. *Int. J. Electr. Comput. Eng.* **2019**, *9*, 3695.
8. Attar, H.H.; Solyman, A.A.; Mohamed, A.E.F.; Khosravi, M.R.; Menon, V.G.; Bashir, A.K.; Tavallali, P. Efficient equalisers for OFDM and DFrFT-OCDM multicarrier systems in mobile E-health video broadcasting with machine learning perspectives. *Phys. Commun.* **2020**, *42*, 101173.
9. Solyman, A.A.; Attar, H.; Khosravi, M.R.; Menon, V.G.; Jolfaei, A.; Balasubramanian, V.; Selvaraj, B.; Tavallali, P. A low-complexity equalizer for video broadcasting in cyber-physical social systems through handheld mobile devices. *IEEE Access* **2020**, *8*, 67591–67602.
10. Sun, Y.; Tong, L. Channel equalization for wireless OFDM systems with ICI and ISI. In Proceedings of the 1999 IEEE International Conference on Communications (Cat. No. 99CH36311), Vancouver, BC, Canada, 6–10 June 1999; Volume 1, pp. 182–186. https://doi.org/10.1109/ICC.1999.767919.
11. Taubock, G.; Hampejs, M.; Svac, P.; Matz, G.; Hlawatsch, F.; Grochenig, K. Low-complexity ICI/ISI equalization in doubly dispersive multicarrier systems using a decision-feedback LSQR algorithm. *IEEE Trans. Signal Process.* **2011**, *59*, 2432–2436.
12. Sherstinsky, A. Fundamentals of recurrent neural network (RNN) and long short-term memory (LSTM) network. *Phys. D Nonlinear Phenom.* **2020**, *404*, 132306.
13. Hochreiter, S.; Schmidhuber, J. Long short-term memory. *Neural Comput.* **1997**, *9*, 1735–1780.
14. Yu, Y.; Si, X.; Hu, C.; Zhang, J. A review of recurrent neural networks: LSTM cells and network architectures. *Neural Comput.* **2019**, *31*, 1235–1270.
15. Farsad, N.; Goldsmith, A. Neural network detection of data sequences in communication systems. *IEEE Trans. Signal Process.* **2018**, *66*, 5663–5678.
16. Ye, H.; Li, G.Y.; Juang, B.H. Power of deep learning for channel estimation and signal detection in OFDM systems. *IEEE Wirel. Commun. Lett.* **2017**, *7*, 114–117.
17. Wang, S.; Yao, R.; Tsiftsis, T.A.; Miridakis, N.I.; Qi, N. Signal detection in uplink time-varying OFDM systems using RNN with bidirectional LSTM. *IEEE Wirel. Commun. Lett.* **2020**, *9*, 1947–1951.
18. Huang, Q.; Zhao, C.; Jiang, M.; Li, X.; Liang, J. A novel OFDM equalizer for large doppler shift channel through deep learning. In Proceedings of the 2019 IEEE 90th Vehicular Technology Conference (VTC2019-Fall), Honolulu, HI, USA, 22–25 September 2019; pp. 1–5.
19. 3GPP TR 38.901. Study on Channel Model for Frequencies from 0.5 to 100 GHz. Technical Specification (ts), 3rd Generation Partnership Project (3GPP), 2020; p. 11. Version 16.1.0. Available online: https://www.etsi.org/deliver/etsi_tr/138900_138999/138901/16.01.00_60/tr_138901v160100p.pdf (accessed on 23 September 2022).
20. 3GPP TS 38.212. 5GNR Multiplexing and Channel Coding. Technical Specification (ts), 3rd Generation Partnership Project (3GPP), 2018; p. 7. Version 15.2.0. Available online: https://www.etsi.org/deliver/etsi_ts/138200_138299/138212/15.02.00_60/ts_138212v150200p.pdf (accessed on 23 September 2022).
21. Cui, T.; Tellambura, C. OFDM channel estimation and data detection with superimposed pilots. *Eur. Trans. Telecommun.* **2011**, *22*, 125–136.
22. Baldi, P.; Sadowski, P.J. Understanding dropout. *Adv. Neural Inf. Process. Syst.* **2013**, *26*. Available online: https://proceedings.neurips.cc/paper/2013/hash/71f6278d140af599e06ad9bf1ba03cb0-Abstract.html (accessed on 23 September 2022).
23. Werbos, P.J. Backpropagation through time: What it does and how to do it. *Proc. IEEE* **1990**, *78*, 1550–1560.
24. Zhang, Z. Improved adam optimizer for deep neural networks. In Proceedings of the 2018 IEEE/ACM 26th International Symposium on Quality of Service (IWQoS), Banff, AB, Canada, 4–6 June 2018; pp. 1–2.

25. Vargas, D.; Elliott, S.; Haffenden, O.; McCartney, R.; Murphy, A.; Jimenez, J.J. Performance of 5G Broadcast and Benefits of Proposed Time-Interleaving Enhancements. IBC Technical Paper; 14 September 2020. Available online: https://www.ibc.org/technical-papers/performance-of-5g-broadcast-and-benefits-of-proposed-time-interleaving-enhancements/6745.article (accessed on 23 September 2022).
26. Sengupta, A.; Alvarino, A.R.; Catovic, A.; Casaccia, L. Cellular Terrestrial Broadcasting—Physical layer evolution from 3GPP release 9 to release 16. *IEEE Trans. Broadcast.* **2020**, *66*, 459–470.